

Optimizing Microstructure and Properties of SiC_f/SiC Composites Prepared by Reactive Melt Infiltration

ZHANG Junmin^{1,2,3}, CHEN Xiaowu^{1,2}, LIAO Chunjin^{1,2}, GUO Feiyu^{1,2,3},
YANG Jinshan^{1,2}, ZHANG Xiangyu^{1,2}, DONG Shaoming^{1,2}

(1. State Key Laboratory of High Performance Ceramics and Superfine Microstructure, Shanghai Institute of Ceramics, Chinese Academy of Sciences, Shanghai 200050, China; 2. Structural Ceramics and Composites Engineering Research Center, Shanghai Institute of Ceramics, Chinese Academy of Sciences, Shanghai 200050, China; 3. School of Physical Science and Technology, Shanghai Tech University, Shanghai 200031, China)

Abstract: Reactive melt infiltration (RMI) is one of the most effective methods to prepare highly dense ceramic matrix composites. The melt infiltration and the formation of composites are mainly determined by the pore structure of preforms. Here, SiC fiber reinforced SiC matrix composites (SiC_f/SiC) were prepared by infiltrating Si melt into carbon-contained preforms with various pore structures. Effects of pore structure on the melt infiltration and received SiC_f/SiC composites were investigated. The results indicated that the preforms with more homogeneous pore size could lead to more sufficient melt infiltration, and also resulted in fewer residual pores and better mechanical properties in the composites. This study is expected to provide important guidance for the pore structure regulation in the fabrication of RMI-composites.

Key words: SiC_f/SiC composites; reactive melt infiltration (RMI); pore structure; microstructure; infiltration kinetics

Due to obvious advantages of fast densification and low cost, reactive melt infiltration (RMI) has become one of the most attractive techniques in the fabrication of ceramic and ceramic-matrix composites^[1-2]. Particularly, increasing research focuses on the fabrication of SiC monolithic and SiC-based composites by RMI method, where Si or Si-based alloy melt is infiltrated into porous carbon preforms and SiC phase is *in-situ* formed through the reaction between them^[3-4]. During RMI process, a porous preform with specific pore structure is constructed, and then a highly reactive melt is infiltrated into the preform, forming the ceramic matrix through the *in-situ* reaction^[5-7]. Both the microstructure and the properties of the received materials can be tailored by adjusting the pore structures of the preforms. This gives high flexibility for RMI method to optimize the obtained materials.

Research proved that melt infiltration kinetics is

strongly dependent on the pore structure of preforms^[8-9]. Washburn equation^[10] indicates that the square of melt infiltration depth is proportional to the pore size. It is worth noting that Washburn equation does not consider the change of pore size. Actually, RMI is a complex process interwoven with melt infiltration and chemical reaction^[11]. For the most basic RMI process of Si melt infiltrating porous carbon to form SiC matrix, the reaction between Si melt and carbon leads to the formation of SiC product layer on the pore wall. The reaction layer thickens gradually with infiltration time, leading to obvious shrinkage and even closure of the pores^[12-13]. Therefore, the reaction can impede the infiltration when the pore closure occurs.

In addition to pore closure, inhomogeneity of pore structure is another important factor affecting the melt infiltration. As for fibrous preforms prepared based on woven fiber bundles, where inter-bundle pores are usually much

Received date: 2021-02-09; **Revised date:** 2021-03-24; **Published online:** 2021-04-05

Foundation item: National Natural Science Foundation of China (51902328); Science and Technology Commission of Shanghai Municipality (19ZR1464700); Innovation Academy for Light-duty Gas Turbine, CAS (CXYJJ20-QN-09); Chinese Academy of Sciences (QYZDY-SSW-JSC031); Key Deployment Project of the Chinese Academy of Sciences (ZDRW-CN-2019-01)

Biography: ZHANG Junmin(1996–), male, PhD candidate. E-mail: zhangjm2@shanghaitech.edu.cn
张俊敏(1996–), 男, 博士研究生. E-mail: zhangjm2@shanghaitech.edu.cn

Corresponding author: CHEN Xiaowu, lecturer. E-mail: xwchen@mail.sic.ac.cn; DONG Shaoming, professor. E-mail: smdong@mail.sic.ac.cn
陈小武, 助理研究员. E-mail: xwchen@mail.sic.ac.cn; 董绍明, 研究员. E-mail: smdong@mail.sic.ac.cn

larger than intra-bundle pores, uniform melt infiltration is hardly realized due to the inhomogeneous pore structure^[14]. Our previous study^[15-16] indicated that the melt infiltrates fibrous preforms roughly by two steps: infiltrates into the inter-bundle pores firstly and then infiltrates the smaller intra-bundle pores. The stepwise melt infiltration caused by the inhomogeneous pore structure can lead to unreacted reactant in the as-received materials. To mitigate the pore structure inhomogeneity of fibrous preform, Zhong *et al*^[17] impregnated carbon fiber preforms with a blend of phenolic resin and pore former, and then fabricated C_f/SiC composites by infiltration of Si melt. The research indicates that sufficient melt infiltration occurs and little unreacted silicon remains as the pore size homogenizes to 1.8 μm . So far, a lot of researches aimed at tailoring the pore structure of preforms to optimize the microstructure and properties of materials^[18-20], while how the pore structure affects the melt infiltration and the final materials still remains un-known.

In present study, SiC fibrous preforms were prepared by slurry impregnation(SI), and the pore structure was adjusted through different impregnation treatments. The effects of pore structure on the melt infiltration and the as-received SiC_f/SiC composites were studied in detail. Compared to phenolic resin impregnation, the preform obtained by polymer blend (organic pore former+phenolic resin) impregnation showed more homogenous pore structure and more sufficient Si melt infiltration, thus resulting in better mechanical properties of the composites. Besides, the infiltration kinetics in terms of pore structure was investigated mathematically, which further con-

firms that the infiltration is controlled by pore structure. This study can provide guidance for optimizing RMI-derived composites by pore structure adjustment.

1 Experimental procedure

1.1 Materials and process

A schematic of material preparation is given in Fig. 1. Firstly, plain-weave KD-II SiC fiber cloths (National University of Defense Technology, China) was coated with BN interphase (~ 500 nm thick) *via* chemical vapor infiltration (CVI) method. SiC slurry prepared by mixing SiC powders was impregnated into SiC fiber cloths by vacuum impregnation. The preparation technology of the slurry is similar with the previous study^[18]. Differently, there were no carbon particles in the slurry, and carbon source was introduced into the preforms by subsequent impregnation treatment. The impregnated fiber cloths were then cut (60 mm \times 60 mm), stacked together (8 layers) and cured at 120 $^{\circ}\text{C}$. The green samples were pyrolyzed at 900 $^{\circ}\text{C}$ in flowing Ar atmosphere to obtain porous preforms.

To obtain preforms with various pore structures, different impregnation treatments were used to adjust the pore structure. The pyrolyzed preforms were divided to three groups: the first group, named Pre-1, was directly densified by RMI without further impregnation, the second group, named Pre-2, was impregnated with phenolic resin (PF; 2130#, Wuxi Guangming Chemical Co. Ltd., Wuxi, China), and the third group was impregnated with a polymer blend of named Pre-3, in which the ratio of organic pore former/PF was 0.2. Then the re-impregnated preforms were cured at 130 $^{\circ}\text{C}$, followed by pyrolysis in flowing Ar atmosphere at 900 $^{\circ}\text{C}$. Finally, Si melt was infiltrated into the preforms at 1490 $^{\circ}\text{C}$ to obtain SiC_f/SiC composites. The designations of the preforms and the composites are shown in Table 1.

Table 1 Different impregnation treatments to the preforms

Preform	Preparing process	Further impregnation	Composites
Pre-1	Slurry impregnation	None	Com-1
Pre-2	Slurry impregnation	Pure PF	Com-2
Pre-3	Slurry impregnation	Polymer blend	Com-3

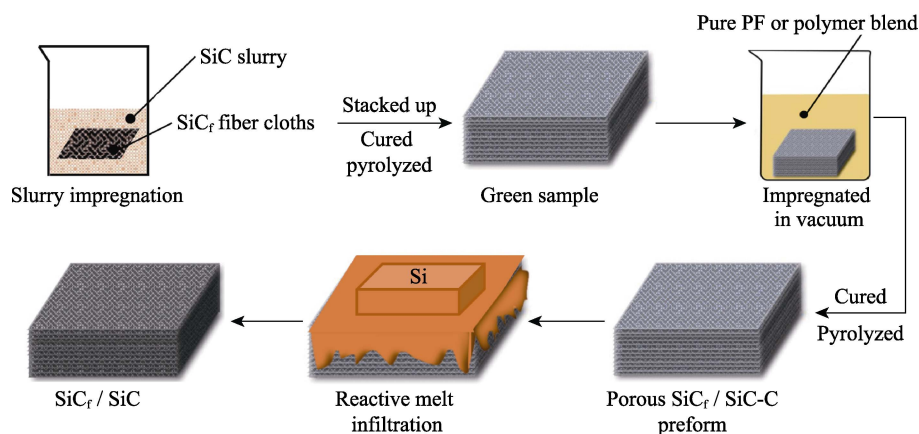


Fig. 1 Flowchart of SiC_f/SiC composites fabrication process

1.2 Tests and characterization

The pore size distribution of the preforms and the porous carbon derived from PF and the polymer blend of organic pore former+PF were analyzed using an AutoPoreIV 9510 mercury porosimeter (Micromeritics, Shanghai, China). The phase compositions of the preforms and the composites were analyzed by a Rigaku D/max X-ray diffractometer (XRD, Rigaku Corporation, Kyoto, Japan) with monochromated Cu-K α radiation (40 kV, 40 mA, 10 (°)·min⁻¹ from 10° to 80°). The microstructures of the preforms and the composites were observed using an S4800 field emission scanning electron microscope (FESEM, Hitachi, Tokyo, Japan). The elemental analyses were conducted by energy dispersive spectroscopy (EDS, Aztec X-Max 20, Oxford, UK).

The bulk density and open porosity of the preforms and the composites were measured by Archimedes method using deionized water as an immersing medium. To evaluate the effects of the preform pore structure on the mechanical properties of the composites, room temperature flexural strength of the composites was determined on specimens with average size of 3 mm×5 mm×40 mm, using a 3-point bending test machine (DDL20, Changchun Research Institute for Mechanical Science Co. Ltd, Changchun, China) with a span of 30 mm and a loading rate of 0.5 mm/min. To minimize the accidental error, at least five specimens were tested, and the reported strength was the averaged value.

2 Results and analysis

To tailor the pore structure of the fibrous preforms, a polymer blend solution of organic pore former and PF was impregnated into the preforms. Fig. 2 shows the microstructure and pore size distributions of the pure PF and the organic pore former-PF blend after the pyrolysis. The pure PF-derived carbon shows a dense structure with few pores (Fig. 2(a)), while the blend-derived carbon consists of interconnected carbon particulates and pore structure. The content of organic pore former has a significant effect on the carbon particulate size and the degree of interconnection. With the increase of organic pore former content, the carbonized product displays more uniform sized carbon particulates (Fig. 2(b-d)). This can be further confirmed by the pore size distributions (Fig. 2(e)). The blend-derived carbon shows micropores with the pore size located between 0.1 and 5 μm . The number of micropores increases significantly with the addition of organic pore former increasing. However, excessive organic pore former significantly increases the viscosity of the blend, resulting in the difficulty of gas escape during the curing process, which causes the abrupt changes of

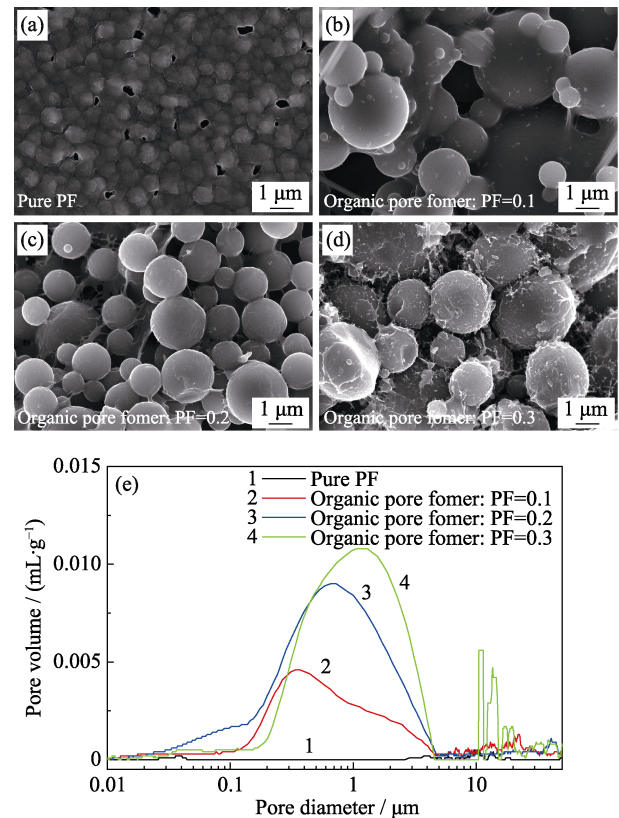


Fig. 2 SEM images of pyrolytic carbon prepared with different organic pore former contents ((a) Pure PF; (b) Organic pore former: PF=0.1; (c) Organic pore former: PF=0.2; (d) Organic pore former: PF=0.3) and (e) Pore size distribution of pyrolytic carbon

the pore volume and inhomogeneous pore size distribution in the pyrolytic carbon. Besides, high viscosity can impede the impregnation of the blend into the preforms. Hence, the optimum ratio of organic pore former/PF in the blend is set at 0.2 in this study.

The microstructures of the preforms with different impregnation treatments (Pre-1, Pre-2, and Pre-3) are shown in Fig. 3(a-c). Pre-1 presents two types of pores: submicron inter-bundle pores and micron intra-bundle pores. The pore volume of Pre-1 changes abruptly was probably due to interlaminar crack appearing in the sample, and the cracks were mistaken for part of the macropore. In the Pre-2 (further impregnation with PF), there are still obvious micropores in the intra-bundles, but the inter-bundle pores are filled or even blocked with the dense pyrolytic carbon. While for Pre-3 (further impregnation with organic pore former+PF blend), the intra-bundle pores are separated into submicron pores, which keeps uniformly with the inter-bundle pores. The pore characteristics of the preforms are further shown in Fig. 3(d). The bimodal pore size distribution of Pre-1 represents the inter-bundle pores and the intra-bundle pores, which indicates the inhomogeneity of pore structure. Pre-2 also shows inhomogeneous pore structure, though the fraction of large-sized

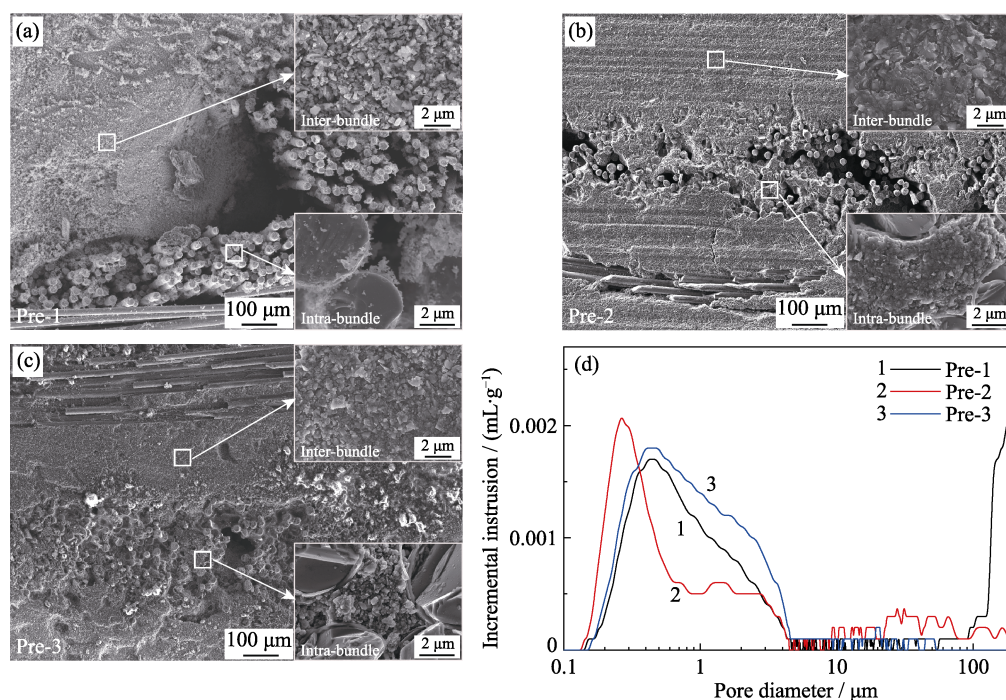


Fig. 3 Cross-sectional SEM images of preforms ((a) Pre-1, (b) Pre-2, (c) Pre-3), and (d) pore size distribution of the preforms

pores in the intra-bundles is significantly reduced. While Pre-3 exhibits homogeneous pore size distribution in the range of 0.1–5.0 μm and large-sized pores almost disappear.

The inhomogeneous pore structure of Pre-1 is caused by the insufficient impregnation of SiC slurry. The fiber bundles are the barrier to the slurry impregnation, leading to massive pores inside the bundles while tiny pores outside the bundles. Repeating impregnation with PF and organic pore former can effectively reduce the pore distribution inhomogeneity. However, the effects of different re-impregnation treatments are significantly different. For pure PF re-impregnation, due to the significant shrinkage of PF during the pyrolysis, the preforms show coexistence of dense carbon and large pores inside the bundles. While for polymer blend (organic pore former+PF) re-impregnation, the shrinkage of PF can be significantly reduced as organic pore former could effectively separate bulk PF into connected island shape. Therefore, the decomposition of organic pore former during the pyrolysis can effectively lead to a homogeneous porous structure. Unlike SiC powder slurry, polymer blend solution can infiltrate inside fiber bundles unimpededly, leaving homogeneous pore structure in the preforms (Pre-3).

After infiltration with Si melt, the preforms (Pre-1, 2, 3) were transformed into SiC_f/SiC composites. Fig. 4 shows XRD patterns of the composites. Four main phases, α -SiC (slurry introduced), β -SiC (reaction formed), Si (infiltration unreacted), and BN (interphase) are detected. The decrease of the BN peak may be related to Si melt

eroding the BN interphase during the RMI. In order to evaluate the effects of preform pore structure on the composite formation, the relative contents of β -SiC/ α -SiC in the composites are calculated based on the intensity ratio of the strongest peaks of β -SiC ($2\theta \approx 35.71^\circ$) and α -SiC ($2\theta \approx 38.18^\circ$). The calculated results of β -SiC/ α -SiC peak ratio in Com-1, Com-2 and Com-3 are 3.12, 4.12 and 5.21, respectively. As the preforms are all impregnated with SiC slurry under the same conditions, the α -SiC contents in all of the preforms can be regarded as identical. Therefore, higher β -SiC/ α -SiC peak ratio means higher β -SiC content. According to the calculation, the β -SiC content is lowest in Com-1 while highest in Com-3. Compared with slurry impregnation (Pre-1) and PF re-impregnation (Pre-2), re-impregnation with polymer blend (organic pore former+PF) can effectively increase the proportion of β -SiC in the composites, sug-

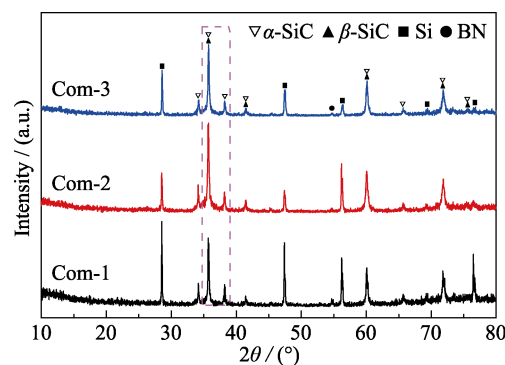


Fig. 4 XRD patterns of SiC_f/SiC composites prepared with different impregnation treatments

gesting that homogenizing the pore structure of the preforms contributes to more sufficient Si infiltration and thus more complete reaction ($\text{Si} + \text{C} \rightarrow \beta\text{-SiC}$).

The microstructures of the composites are shown in Fig. 5. There are fewer residual intra-bundle pores in Com-3, but massive pores in Com-1 and Com-2. This can be attributed to the different pore structures in the preforms. Due to the bimodal pore size distribution (corresponding to inter/intra-bundle pores) in Pre-1 and Pre-2, the preforms can be approximated as the “narrow-mouth bottle”. Therefore, Si melt infiltration in the preforms is a step-wise process: infiltrating into inter-bundle pores (narrow mouth of bottle) firstly and then infiltrating into intra-bundle pores (wide body of bottle). Small inter-bundle pores will greatly limit the speed of Si melt infiltrating into the intra-bundle pores, and large intra-bundle pores increase the difficulty of Si melt densifying the intra-bundle matrix. Hence, the nonuniform pore structure is obviously not conducive to the infiltration kinetics inside the fiber bundles. Especially the volume expansion effect of reaction between Si and C contribute to premature blockage of inter-bundle pores, leading to insufficient melt infiltrating into intra-bundle pores in Com-2. While Pre-3 exhibits homogeneous pore size distribution with smaller intra-bundle pores and larger inter-bundle pores than Pre-2. Smaller intra-bundle pores benefit the rapid densification of the matrix inside bundles fibers, and larger inter-bundle pores slow down the closure of pores, leading to more sufficient infiltration of Si melt and less residual pores.

In order to further investigate the effects of inter/intra-bundle pores on the composite formation, element compositions of the composites were analyzed (Fig. 6). The Si/C atomic ratio in inter/intra-bundle of Com-3 is approximately 1, while that of Com-1 is remarkably higher than 1. This indicates that relatively higher Si residue content in Com-1 than that in Com-3, which is consistent with the results shown in Fig. 4. Interestingly, for Com-2, Si residue is mainly located at the inter-bundles according to the Si/C ratio in inter/intra-bundles. The fact mentioned that no carbon is introduced into Pre-1, where

the Si melt infiltration is nonreactive. Hence more residual Si exists in intra-bundles with massive pores in Com-1. While the Si melt infiltration in Pre-2 is reactive, too small inter-bundles pores limit Si melt infiltrating into the intra-bundle pores, resulting in more residual Si outside bundles fibers in Com-2. Homogeneous pore structure of Pre-3 leads to homogeneous Si melt infiltration. This verifies that pore structure of preforms decides the phase composition of the composites, and homogeneous pore structure between inter/intra-bundles facilitates sufficient melt infiltration and complete reaction between Si and C.

Three-point bending tests were performed to contrast the mechanical properties of the composites. The mechanical properties are summarized in Table 2, and load-displacement curves as well as fracture surfaces are shown in Fig. 7. All composites show a typical pseudo-plastic fracture behavior (Fig. 7(a)). Com-3 shows the highest bending strength, while Com-1 shows the lowest bending strength. The different mechanical properties should be attributed to the different melt infiltration modes. As discussed above, Com-1 has massive residual pores in the intra-bundle (Fig. 5(a)) due to the insufficient melt infiltration, which almost contributes to no bonding between the fiber and the matrix. The absence of bonding makes stress transfer between fiber/matrix unattainable, resulting in few fibers pulling off matrix on the fracture surface (Fig. 7(b)). Com-2 and Com-3 show significant fiber pull-out on the fracture surfaces (Fig. 7(c-d)). Benefiting from dense matrix in inter/intra bundle, Com-3 shows independent and gradual fiber pull-out, which is favorable for crack propagation and stress relaxation. This fracture mechanism can maximize the reinforcing effect of the fibers, thus endowing the composite with higher mechanical strength. Besides, Chen *et al.*^[16] prepared the preform with more uniform pore size distribution by sol impregnation than that by slurry impregnation (SI), and the composite prepared by sol impregnation shows higher flexural strength (192 MPa) than that by slurry impregnation (145 MPa). Zhong *et al.*^[17] improved the homogeneity of preform by using pore former and the composite obtained a tensile strength of (159 ± 5) MPa, which

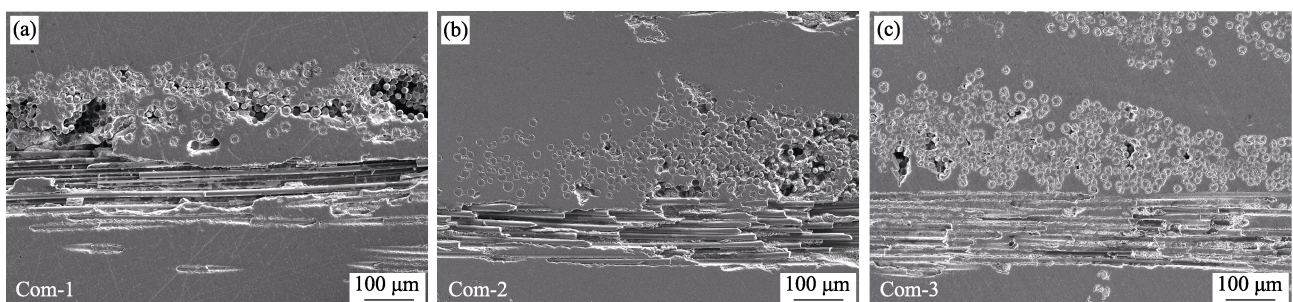


Fig. 5 Cross-sectional SEM images of SiC_f/SiC
(a) Com-1, (b) Com-2 and (c) Com-3

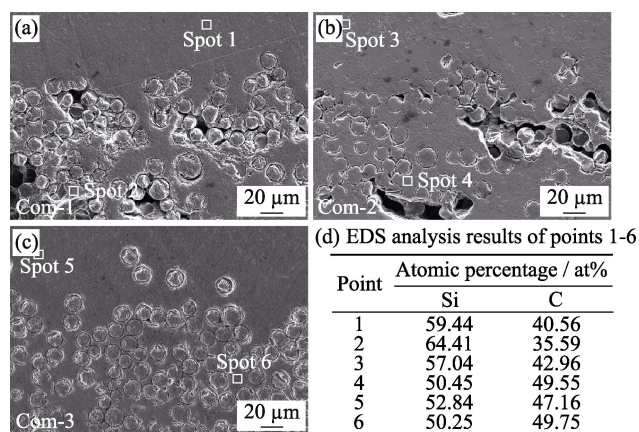


Fig. 6 Elemental analyses of inter/intra-bundle matrix in composites

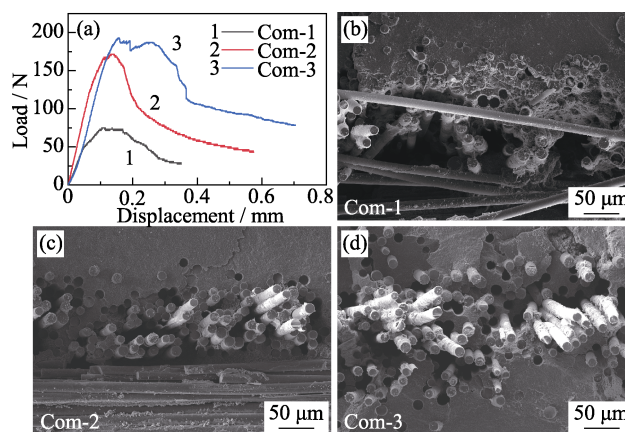


Fig. 7 (a) Bending load-displacement curves of composites, and fractural surface SEM images of composite ((b) Com-1, (c) Com-2 and (d) Com-3)

Table 2 Comparison of the mechanical properties of the SiC_f/SiC composites

Composites	Density/(g·cm ⁻³)	Open porosity/%	Flexural strength/MPa	Elastic modulus/GPa
Com-1	(2.41±0.08)	(10.08±0.50)	(96.04±9.50)	(42.53±0.73)
Com-2	(2.57±0.08)	(8.39±0.58)	(176.76±3.78)	(67.55±0.46)
Com-3	(2.61±0.05)	(7.92±0.61)	(200.50±7.33)	(79.19±0.65)

was 46% higher than that without pore former. These researches also verify that homogeneous pores structure of preform is beneficial to the mechanical properties of the received RMI-composite.

For RMI-composites, the matrix formation and the mechanical behavior are closely related with the pore structure of preforms, as the pore structure directly decides the melt infiltration kinetics. Therefore, establishing the mathematical relationship between the infiltration kinetics and the pore structure is extremely essential to optimize the composites. For RMI SiC_f/SiC composites, pore size reduction caused by β -SiC layer formed on the pore wall ($\text{Si}+\text{C}\rightarrow\beta\text{-SiC}$) is the key process to control the infiltration kinetics (Fig. 8(a)). Assuming that the growth of β -SiC layer is a diffusion-limited process, then the relationship between pore size and infiltration time can be expressed as^[21]:

$$t = \frac{M_{\text{Si}} \cdot \rho_{\text{SiC}} \cdot r_0^2}{6M_{\text{SiC}} \cdot \rho_{\text{Si}} \cdot D_{\text{C/SiC}}} \left[1 - 3 \left(\frac{r_t}{r_0} \right)^2 + 2 \left(\frac{r_t}{r_0} \right)^3 \right] \quad (1)$$

where M_{Si} , M_{SiC} , ρ_{Si} and ρ_{SiC} are the molar weights and densities of Si melt and reaction layer (β -SiC), respectively. $D_{\text{C/SiC}}$ is the theoretical diffusion coefficient of C atom in the reaction layer, and r_0 and r_t are the initial ($t=0$) and final pore radii of the preform.

Substituting $M_{\text{Si}}=28.1$ g/mol, $M_{\text{SiC}}=40.1$ g/mol, $\rho_{\text{Si}}=2.33$ g/cm³, $\rho_{\text{SiC}}=3.21$ g/cm³ and $D_{\text{C/SiC}}=1.98 \times 10^{-12}$ cm²/s^[22], Eq. (1) can be written as below.

$$t = 812.63 \times r_0^2 \left[1 - 3 \left(\frac{r_t}{r_0} \right)^2 + 2 \left(\frac{r_t}{r_0} \right)^3 \right] \quad (2)$$

For preforms with inhomogeneous pore structures, r_0 can be assumed as the median pore radius obtained from mercury porosimeter, which corresponds to the pore radius at cumulative volume percentage reaching 50%. As discussed previously, the inter-bundle pores (0–10 μm) in the preforms play more critical role in the melt infiltration. Hence, it is more appropriate to calculate the median pore radius of the inter-bundle pores. The cumulative volume percentages *versus* the pore diameter within 0–10 μm are shown in Fig. 8(b). As Pre-1 is obtained by SiC slurry infiltration without any carbon addition, the melt infiltration in the preform is a non-reactive mode, which makes it inadequate to the equation above. Therefore, only infiltration kinetics of Pre-2 and Pre-3 are calculated.

Substituting Pre-2: $r_0=0.21$ μm, Pre-3: $r_0=0.33$ μm. Then Eq. 3 can be written as below.

$$\text{Pre-2: } t = 35.84 \left[1 - 3 \left(\frac{r_t}{0.21} \right)^2 + 2 \left(\frac{r_t}{0.21} \right)^3 \right] \quad (3)$$

$$\text{Pre-3: } t = 88.50 \left[1 - 3 \left(\frac{r_t}{0.33} \right)^2 + 2 \left(\frac{r_t}{0.33} \right)^3 \right] \quad (4)$$

According to Eq. (3) and (4), the curves of pore radius (r) *versus* infiltration time (t) are obtained, as shown in Fig. 8(c).

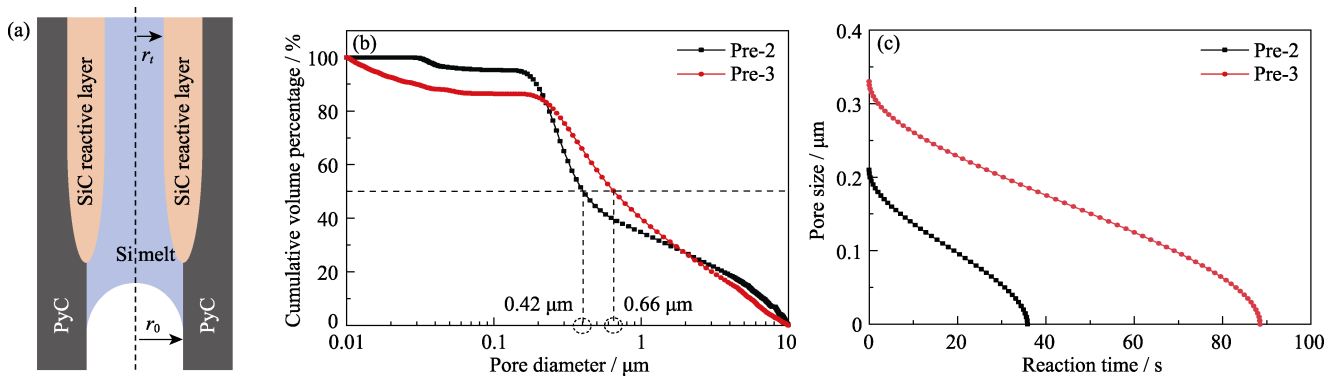


Fig. 8 (a) Schematic of reaction layer generated during the RMI, (b) curves of cumulative volume percentage vs pore diameter of preforms, and (c) variation of pore radius with infiltration time for preforms

The calculation results indicate that pore size of the preforms decreases quickly with the infiltration going on. The decrease of pore size increases the viscous resistance between the melt and the pore wall, impeding the melt infiltration. When the pore size decreases to zero (pore closure), the infiltration kinetics is suppressed dramatically. For Pre-2, the time that pore radius decreases to zero is about 36 s, while that for Pre-3 is 89 s. Longer time the pore closure needs, more favorable kinetically the melt infiltration is. The time of pore closure in Pre-3 is about 2.5 times of that of Pre-2, resulting in more sufficient melt infiltration in Pre-3. This leads to denser matrix and better mechanical properties in the Com-3. As the calculation simplifies the pore structures, the results may deviate the real situation. However, as one of rare attempts to reveal melt infiltration kinetics from the view of pore structure, the present study is expected provide important guidance for pore structure regulation in the fabrication of melt-infiltrated composites.

3 Conclusion

The SiC_f/SiC composites were fabricated by Si melt infiltration into porous preforms. The pore structure of the preforms was adjusted by SiC slurry impregnation and subsequent polymer re-impregnation. The effects of pore structure on the melt infiltration and the obtained composites were studied. The results indicate that the preforms impregnated with polymer blend (organic pore former+PF) show much more homogeneous pore structure compared with those impregnated with SiC slurry and PF. The homogeneous pore structure leads to more sufficient Si melt infiltration and denser ceramic matrix in the composites, as well as better mechanical properties. Besides, the melt infiltration kinetics in terms of pore structure was calculated, indicating that the pore size decreases quickly with the infiltration going on. As the time needed for pore closure in organic pore former+PF impregnated preforms is longer than that for PF

impregnated preform, this makes infiltration kinetics more favorable and thus leads to more sufficient melt infiltration and better mechanical properties in the former.

References:

- [1] ZHU Y, WANG S, LI W, *et al.* Preparation of carbon fiber-reinforced zirconium carbide matrix composites by reactive melt infiltration at relative low temperature. *Scripta Materialia*, 2012, **67**(10): 822–825.
- [2] WANG J, LIN M, XU Z, *et al.* Microstructure and mechanical properties of C/C-SiC composites fabricated by a rapid processing method. *J. Eur. Ceram. Soc.*, 2009, **29**(14): 3091–3097.
- [3] TIAN J T, SHOBU K. Fabrication of silicon carbide-mullite composite by melt infiltration. *J. Am. Ceram. Soc.*, 2003, **86**(1): 39–42.
- [4] SINGH M, ALMAN D E, HAWK J A. Microstructure and Wear Behavior of SiC-based Composites Fabricated by Melt Infiltration, in: Alman D E, HAWK J A., SIMMONS J W (Eds.). *Roll of Characterization in Understanding Environmental Degradation of Materials*, ASM International, 1998: 169–175.
- [5] WANG Y X, TAN S H, JIANG D L. The effect of porous carbon preform and the infiltration process on the properties of reaction-formed SiC. *Carbon*, 2004, **42**(8/9): 1833–1839.
- [6] JIANG S Z, XIONG X, CHEN Z K, *et al.* Influence factors of C/C-SiC dual matrix composites prepared by reactive melt infiltration. *Materials & Design*, 2009, **30**(9): 3738–3742.
- [7] WANG D, DONG S M, ZHOU H J, *et al.* Fabrication and microstructure of 3D C_f/ZrC-SiC composites: through RMI method with ZrO₂ powders as pore-making agent. *Ceram. Int.*, 2016, **42**(6): 6720–6727.
- [8] ROGER J, CHOLLON G. Mechanisms and kinetics during reactive infiltration of molten silicon in porous graphite. *Ceram. Int.*, 2019, **45**(7): 8690–8699.
- [9] PILLLEE S, KIYOON H, SOOPARK J, *et al.* Processing and properties of SiC and SiC/SiC composite materials by melt infiltration process. *International Journal of Modern Physics B*, 2003, **17**(8): 1833–1838.
- [10] WASHBURN E W. The dynamics of capillary flow. *Physical Review*, 1921, **17**(3): 273–283.
- [11] BOUGIOURI V, VOYTOVYCH R, ROJO-CALDERON N, *et al.* The role of the chemical reaction in the infiltration of porous carbon by NiSi alloys. *Scripta Materialia*, 2006, **54**(11): 1875–1878.
- [12] KUMAR S, KUMAR A, SHUKLA A, *et al.* Capillary infiltration studies of liquids into 3D-stitched C-C preforms Part A: Internal

- pore characterization by solvent infiltration, mercury porosimetry, and permeability studies. *J. Eur. Ceram. Soc.*, 2009, **29**(12): 2643–2650.
- [13] KUMAR S, KUMAR A, DEVI R, *et al.* Capillary infiltration studies of liquids into 3D-stitched C-C preforms Part B: Kinetics of silicon infiltration. *J. Eur. Ceram. Soc.*, 2009, **29**(12): 2651–2657.
- [14] WANG Y, ZHU X, ZHANG L, *et al.* C/C-SiC-ZrC composites fabricated by reactive melt infiltration with $\text{Si}_{0.87}\text{Zr}_{0.13}$ alloy. *Ceram. Int.*, 2012, **38**(5): 4337–4343.
- [15] CHEN X W, NI D W, KAN Y M, *et al.* Reaction mechanism and microstructure development of ZrSi_2 melt-infiltrated C_f/SiC -ZrC-ZrB₂ composites: the influence of preform pore structures. *Journal of Materiomics*, 2018, **4**(3): 266–275.
- [16] CHEN X W, FENG Q, KAN Y M, *et al.* Effects of preform pore structure on infiltration kinetics and microstructure evolution of RMI-derived C_f/SiC -ZrC-ZrB₂ composite. *J. Eur. Ceram. Soc.*, 2020, **40**(7): 2683–2690.
- [17] ZHONG Q, ZHANG X Y, DONG S M, *et al.* Reactive melt infiltrated C_f/SiC composites with robust matrix derived from novel engineered pyrolytic carbon structure. *Ceram. Int.*, 2017, **43**(7): 5832–5836.
- [18] LEE S P, PARK J S, KATOH Y, *et al.* Process, microstructure and flexural properties of reaction sintered Tyranno SA/SiC composites. *Journal of Nuclear Materials*, 2002, **307**: 1191–1195.
- [19] ZHAO Y Y, XIA H Y, TANG R, *et al.* A low cost preparation of C/SiC composites by infiltrating molten Si into gelcasted pure porous carbon preform. *Ceram. Int.*, 2015, **41**(5): 6478–6487.
- [20] SINGH M, FARMER S C. Morphological characterization of microporous carbon materials. *Journal of Materials Science Letters*, 1997, **16**(11): 946–949.
- [21] LEVENSPIEL O. *Ingeniería de las Reacciones*. 2nd ed. Wiley (ed.). Barcelona: Revertre, 1978.
- [22] HON M H, DAVIS R F. Self-diffusion of C-14 in polycrystalline beta-sic. *J. Mater. Sci.*, 1979, **14**(10): 2411–2421.

SiC_f/SiC 复合材料的 RMI 制备方法以及微观结构和性能优化

张俊敏^{1,2,3}, 陈小武^{1,2}, 廖春景^{1,2}, 郭斐宇^{1,2,3},
杨金山^{1,2}, 张翔宇^{1,2}, 董绍明^{1,2}

(1. 中国科学院 上海硅酸盐研究所, 高性能陶瓷和超微结构国家重点实验室, 上海 200050; 2. 中国科学院 上海硅酸盐研究所, 结构陶瓷及复合材料工程研究中心, 上海 200050; 3. 上海科技大学 物理科学与技术学院, 上海 200031)

摘 要: 反应熔体渗透(RMI)是制备高密度陶瓷基复合材料的有效方法之一, 而熔体的渗透和复合材料的形成主要取决于预制体的孔隙结构。本研究将硅熔体渗透到具有不同孔隙结构的含碳预制体中, 制备了 SiC 纤维增强 SiC 基复合材料(SiC_f/SiC), 并研究了孔隙结构对熔体浸润和 SiC_f/SiC 复合材料的影响。研究表明: 具有较均匀孔径的预制体可以使熔体浸润更充分, 制备的复合材料具有更少的残余孔隙及更优的力学性能。该研究对反应熔体渗透复合材料的孔结构调控具有指导意义。

关 键 词: SiC_f/SiC 复合材料; 反应熔体渗透(RMI); 孔隙结构; 微观结构; 熔渗动力学

中图分类号: TQ174 文献标志码: A